ISABE-2015-20128

FAST MULTIAXIAL HIGH CYCLE FATIGUE EVALUATION IN THE PROBABILISTIC FATIGUE POST-PROCESSOR AROMA-PF

Daniel Sandberg
KTH Royal Institute of Technology
Department of Solid Mechanics
SE - 100 44 Stockholm, Sweden

Salar Sadek
KTH Royal Institute of Technology
Department of Solid Mechanics
SE - 100 44 Stockholm, Sweden

Gunnar Högström
GKN Aerospace Engine Systems
SE – 461 81 Trollhättan, Sweden

Mårten Olsson
KTH Royal Institute of Technology
Department of Solid Mechanics
SE - 100 44 Stockholm, Sweden

Abstract

The probabilistic high cycle fatigue (HCF) post-processor AROMA-PF, developed mainly for HCF design of compressor blades, is presented. Several local multiaxial HCF criteria have been implemented for computation of the fatigue effective stress, and two volume based probabilistic HCF models have been implemented for computation of the fatigue probability: Weakest-link (WL) and the Volume method for the Probability of Fatigue (VPF). It is shown that for the type of stress history that acts in a compressor blade, for stress invariant based criteria, the effective stress can be expressed in closed form. This enables fast HCF evaluations. By comparing WL and VPF to test data obtained for Ti-6-4 specimens, it is seen that the highest transferability is obtained for WL used in combination with Crossland´s HCF criterion. The results also indicate on that the true fatigue behavior at low p_f-values is between the predictions obtained by use of WL and VPF.

Nomenclature

b	Weibull exponent
f	frequency
$\mathbf{I}$	identity tensor
J	determinant of the Jacobi matrix
J_2	2nd invariant of the stress deviation tensor
k	number of failed specimens
K_t	stress concentration factor
n	number of tested specimens
p_f	failure probability
p_f'	failure probability density
q	material parameter in VPF
$\boldsymbol{s}$	stress deviation tensor
$\boldsymbol{S}$	stress vector
$t, \boldsymbol{x}$	time, position
V	material volume
V_0	reference volume
V^*	highly stressed volume
V_{th}	threshold volume
w	Gauss point weight
α	weight factor in HCF criteria
η	safety factor
$\boldsymbol{\sigma}$	stress tensor
σ_0	characteristic fatigue strength
σ_1	1st (maximum) principal stress
σ_{eff}	fatigue effective stress
σ_{h}	hydrostatic stress
σ_{th}	threshold stress
ω	angular frequency

Subscripts

amp	amplitude
alt	alternating
c	critical
C,S	Crossland, Sines

Superscripts

exp	experimental
Im	imaginary
Re	real
tot	total

1. Introduction

Many components in turbomachinery, such as compressor blades, are subjected to high cycle fatigue (HCF) due to vibrations. State-of-the-art in HCF design is the deterministic point stress method. At each point $\boldsymbol{x}$ in the component, a local multiaxial HCF criterion is used to transform the multiaxial stress history $\boldsymbol{\sigma}(\boldsymbol{x},t)$ into a fatigue effective stress $\sigma_{\text{eff}}(\boldsymbol{x})$. To avoid fatigue, the effective stress at each point $\boldsymbol{x}$ should be below a certain critical effective stress value, $\sigma_{\text{eff,c}}$, including a safety factor η. The design criterion is formulated according to

$$\sigma_{\text{eff,max}_{\boldsymbol{x}}}(\eta) < \sigma_{\text{eff,c}}\,. \qquad (1)$$

The safety factor η is used to account for different type of uncertainties, for example variation in: Material strength, loading, manufacturing, assembly and handling.

For computation of the fatigue effective stress field $\sigma_{\text{eff}}(\boldsymbol{x})$, several HCF criteria can be used. The criteria are phenomenological based models, and they combine different stresses. Typically, the effective stress $\sigma_{\text{eff}}(\boldsymbol{x})$ is computed by adding a weighted normal/hydrostatic stress measure to the shear stress amplitude. There exist criteria based on the critical plane approach (*e.g.* Findley[1], Matake[2] or Dang Van[3]), and criteria based on stress invariants (*e.g.* Sines[4] or Crossland[5]), see Section 2. Use of a critical plane criterion typically involves a time consuming search for the critical plane at each material point $\boldsymbol{x}$. In an industrial situation, where the computational time is critical for the choice of HCF criterion, the stress invariant based criteria are popular. The stress invariant based criteria are originally formulated for stress histories where the varying part of the stress is proportional and where the extreme values of all the stress components occur at the same times during the load cycle. However, in a compressor blade, due to differences in phase between the stress components, the varying part of the stress history is non-proportional, and the extreme values of the stress components do not occur at the same times. Various methods that enable use of the stress invariant based criteria for general stress histories have been suggested. One such method is the minimum circumscribing hypersphere method[8] (MCH). In Section 3, it is shown that when MCH is used, for the type of stress history that acts in a compressor blade, the effective stress $\sigma_{\text{eff}}(\boldsymbol{x})$ computed by use of a stress invariant based criterion can be expressed in closed form.

In traditional HCF design, no efforts are made to model the uncertainties in the design setup. Instead, the overall uncertainty is handled by use of the safety factor η, typically chosen based on engineering experience. A current development is to identify and model the uncertainties in the design setup, see Figure 1.

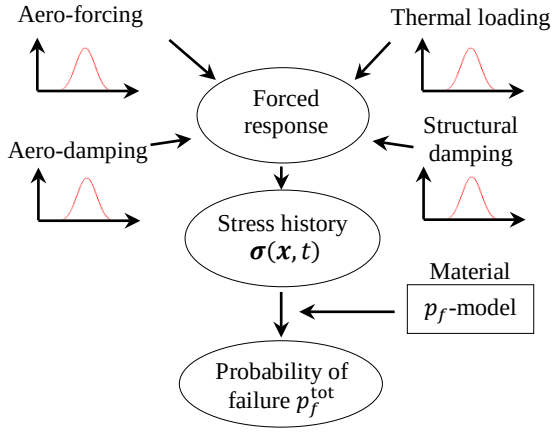

Figure 1. Example of uncertainties modelled in the design setup for a compressor blade.

The aim is to compute the probability of failure, p_f^{tot}. Modelling the uncertainties in the design setup gives improved description of safety, and it is possible to identify the sources of fatigue and manage them.

For many materials, randomly distributed defects are critical for fatigue crack initiation. The defects can be of different types: Particles, voids, inclusions, etc. To model the inherent uncertainty in the fatigue properties of the material, usually weakest-link theory[6,7] (WL) is used. WL theory is based on the assumption that defects that are statistically independent and randomly distributed in position, orientation and size are the cause of fatigue crack initiation. Based on the effective stress field $\sigma_{\text{eff}}(\boldsymbol{x})$, the failure probability, p_f, for a component with volume V is given by

$$p_f = 1 - \exp\left[-\frac{1}{V_0}\int_V \left(\frac{\langle\sigma_{\text{eff}}(\boldsymbol{x})-\sigma_{\text{th}}\rangle}{\sigma_0}\right)^b dV\right], \quad (2)$$

where the Weibull exponent b, the characteristic fatigue strength σ_0 and the threshold stress σ_{th} are material parameters estimated from fatigue test data. The Macaulay brackets, $\langle x\rangle$, is zero if the argument is negative, and x for positive arguments. The reference volume V_0 is arbitrarily chosen (and σ_0 is adjusted accordingly). Eq. 2 models the inherently probabilistic fatigue behavior. In WL, the higher stressed a material point is, the more that material point contributes to p_f. Also, since the failure probability p_f is computed from a volume integration, if the number of highly stressed points increases, even if the maximum stress in the component is the same, the predicted failure probability increases. This means that even large regions of medium high stress may give a significant contribution to the failure probability for a component. The effect is known as the *volume effect*. In the deterministic point stress method, since fatigue prediction is based only on the maximum effective stress, see Eq. 1, the volume effect is not accounted for. For compressor blades, where the effective stress field distribution may be significantly different depending on the shape of the excited mode, the volume effect is important to consider in the fatigue prediction.

The deterministic point stress method and WL are totally different types of models. The state-of-the-art deterministic method gives a yes/no answer to fatigue, while the latter is used to, given a specific stress history, account for uncertainty in the material's fatigue properties, and compute the probability of fatigue, p_f.

In order to enable use of probabilistic HCF models in design of compressor blades, the HCF post-processor AROMA-PF (Aeroelastic Reduced Order Modelling Analysis – Probability of Failure) has been developed, see Section 4. The program uses data generated by use of a commercial FE-software as input. A number of local HCF criteria have been implemented for computation of the fatigue effective stress field $\sigma_{\text{eff}}(\boldsymbol{x})$. Two probabilistic HCF models have been implemented in AROMA-PF: The WL model in Eq. 2, and the newly developed Volume method for the Probability of Fatigue (VPF), presented in Section 4.

In Section 5, experimental data obtained for Ti-6-4 is used to investigate the transferability for WL and VPF. Transferability is a general concept of prediction accuracy in between different geometries. Finally, in Section 6, it is illustrated how AROMA-PF is applied to a compressor blade geometry for computation of p_f.

2. Local multiaxial HCF criteria

In total, five local multiaxial HCF criteria used for computation of the fatigue effective stress, $\sigma_{\text{eff}}(\boldsymbol{x})$, have been implemented in AROMA-PF. Among them are two stress invariant based criteria (Sines and Crossland) and three critical plane criteria (Findley, Matake and Dang Van).

Sines´ criterion is formulated for stress histories where the alternating part of the stress is proportional, *i.e.* where the extreme values of each stress component occur at the same times, $t = t_1$ and $t = t_2$, during the load cycle. The times $t = t_1$ and $t = t_2$ are times for maximum and minimum load, respectively, or vice versa. According to Sines, at a point $\boldsymbol{x}$, the effective stress is computed according to

$$\sigma_{\text{eff,S}} = \sqrt{J_{2,\text{amp}}} + \alpha_{\text{S}} \cdot \sigma_{\text{h,mean}}, \qquad (3)$$

where α is a material parameter that controls the influence of the hydrostatic mean stress $\sigma_{\text{h,mean}}$ on the effective stress $\sigma_{\text{eff,S}}$, and $\sqrt{J_{2,\text{amp}}}$ is the square root of the amplitude of the second invariant of the stress deviation tensor $\boldsymbol{s}_{\text{alt}} = \boldsymbol{\sigma}_{\text{alt}} - \frac{1}{3}\mathbf{I} \cdot \text{tr}(\boldsymbol{\sigma}_{\text{alt}})$. In the original formulation of Sines´ criterion, $\sqrt{J_{2,\text{amp}}}$ is defined according to

$$\sqrt{J_{2,\text{amp}}} = \sqrt{J_2(\boldsymbol{\sigma}_{\text{alt}})}, \qquad (4)$$

where each element in the tensor $\boldsymbol{\sigma}_{\text{alt}}$ is computed according to

$$\sigma_{\text{alt},ij} = \frac{\sigma_{ij}(t=t_1) - \sigma_{ij}(t=t_2)}{2}. \qquad (5)$$

The hydrostatic mean stress $\sigma_{\text{h,mean}}$ is computed as

$$\sigma_{\text{h,mean}} = \frac{\sigma_{\text{h,max}} + \sigma_{\text{h,min}}}{2}. \qquad (6)$$

Crossland´s criterion is similar to Sines´ criterion, but instead of the mean hydrostatic stress, the maximum hydrostatic stress that acts at a point $\boldsymbol{x}$ during the load cycle is used for computation of the fatigue effective stress,

$$\sigma_{\text{eff,C}} = \sqrt{J_{2,\text{amp}}} + \alpha_{\text{C}} \cdot \sigma_{\text{h,max}}. \qquad (7)$$

Here, the critical plane criteria are not presented in detail.

3. Stress invariant based HCF criteria applied to a compressor blade

The stress history that acts in a compressor blade typically consists of a mean stress, $\boldsymbol{\sigma}_{\text{mean}}$, caused mainly by rotation, and a varying stress caused by aerodynamically induced blade vibrations. At a point $\boldsymbol{x}$, each stress component in the stress tensor $\boldsymbol{\sigma}(\boldsymbol{x}, t)$ can be written according to

$$\sigma_{ij}(\boldsymbol{x}, t) = \sigma_{\text{mean},ij}(\boldsymbol{x}) + \sigma^{\text{Re}}_{\text{amp},ij}(\boldsymbol{x})\cos(\omega t) + \sigma^{\text{Im}}_{\text{amp},ij}(\boldsymbol{x})\sin(\omega t). \qquad (8)$$

The stress tensors $\boldsymbol{\sigma}^{\text{Re}}_{\text{amp}}$ and $\boldsymbol{\sigma}^{\text{Im}}_{\text{amp}}$ are used to describe the varying part of the total stress, and the difference in phase between the stress components. At a point $\boldsymbol{x}$, due to the difference in phase between the stress components, the extreme values of the stress components do not occur at the same times $t = t_1$ and $t = t_2$ during the load cycle. Therefore, Eq. 4 and Eq. 5 are not applicable for computation of $\sqrt{J_{2,\text{amp}}}$. One method that has been suggested for computation of $\sqrt{J_{2,\text{amp}}}$ for a general stress history is the MCH[8]. Firstly, the six stress deviator components (five independent) are transformed into a vector $\boldsymbol{S}$ of a five dimensional space R_5, where

$$S_1 = \frac{\sqrt{3}}{2} s_{xx};\ S_2 = \frac{1}{2}\left(s_{yy} - s_{zz}\right);\quad S_3 = s_{xy};\ S_4 = s_{xz};\ S_5 = s_{yz}. \qquad (9)$$

The relation $\sqrt{J_2} = \|\boldsymbol{S}\|$ holds, *i.e.* the length of vector $\boldsymbol{S}$ in R_5 equals to $\sqrt{J_2}$. The stress measure $\sqrt{J_{2,\mathrm{amp}}}$ is defined as the radius of the smallest hyper-sphere that encloses the deviatoric stress path,

$$\sqrt{J_{2,\mathrm{amp}}} = \min_{\boldsymbol{S}'} \{\max_t \|\boldsymbol{S}(t) - \boldsymbol{S}'\|\}, \quad \boldsymbol{S}_{\mathrm{mean}} \tag{10}$$

where $\boldsymbol{S}_{\mathrm{mean}}$ is the center point of the hypersphere. The mean stress, $\boldsymbol{\sigma}_{\mathrm{mean}}$, in Eq. 8 only affects the translation of a hyper-sphere in R_5. It is the tensors $\boldsymbol{\sigma}_{\mathrm{amp}}^{\mathrm{Re}}$ and $\boldsymbol{\sigma}_{\mathrm{amp}}^{\mathrm{Im}}$ that control the radius of the sphere. At point $\boldsymbol{x}$, for the stress history given in Eq. 8, the expression for $\sqrt{J_{2,\mathrm{amp}}}$ given in Eq. 10 can be written according to

$$\sqrt{J_{2,\mathrm{amp}}} = \max_t \left[\sqrt{J_2\left(\boldsymbol{\sigma}_{\mathrm{amp}}^{\mathrm{Re}} \cos(\omega t) + \boldsymbol{\sigma}_{\mathrm{amp}}^{\mathrm{Im}} \sin(\omega t)\right)} \right]. \tag{11}$$

The stress $\sqrt{J_2\left(\boldsymbol{\sigma}_{\mathrm{amp}}^{\mathrm{Re}} \cos(\omega t) + \boldsymbol{\sigma}_{\mathrm{amp}}^{\mathrm{Im}} \sin(\omega t)\right)}$ can be expressed as

$$\sqrt{J_2\left(\boldsymbol{\sigma}_{\mathrm{amp}}^{\mathrm{Re}} \cos(\omega t) + \boldsymbol{\sigma}_{\mathrm{amp}}^{\mathrm{Im}} \sin(\omega t)\right)} = (1/\sqrt{3}) \cdot \sqrt{A \cdot \cos^2(\omega t) + B \cdot \sin^2(\omega t) + C \cdot \cos(\omega t) \cdot \sin(\omega t)}, \tag{12}$$

where the constants A, B and C are computed by use of the relevant components in the tensors $\boldsymbol{\sigma}_{\mathrm{amp}}^{\mathrm{Re}}$ and $\boldsymbol{\sigma}_{\mathrm{amp}}^{\mathrm{Im}}$. Differentiation of Eq. 12, and setting $\frac{d(\sqrt{J_2})}{dt} = 0$, enables computation of $\sqrt{J_{2,\mathrm{amp}}}$ without time search of the load cycle. This gives extra fast computations of the fatigue effective stress for the stress invariant based criteria.

4. The HCF post-processor AROMA-PF

The HCF post-processor AROMA-PF is written in Matlab, and the structure of the program is presented in Figure 2.

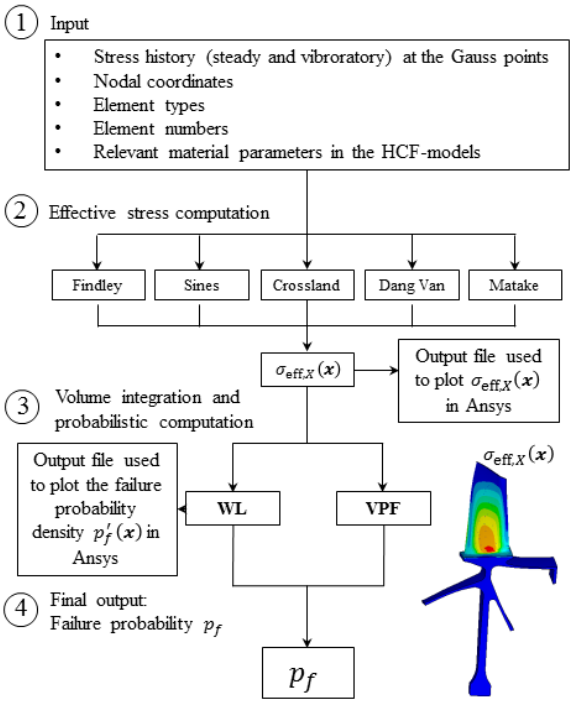

Figure 2. The HCF post-processor AROMA-PF.

The stress input is generated from a commercial FE software and is the steady, real and imaginary stress, see Eq. 8, that acts at the elements´ Gauss points. The effective stress, $\sigma_{\mathrm{eff}}(\boldsymbol{x})$, is computed at each Gauss point by use of one of the implemented local HCF criteria. For the stress invariant based criteria, the $\sqrt{J_{2,\mathrm{amp}}}$ computation is performed by use of the analytical solution to MCH given in Section 3. During a run in AROMA-PF, when the effective stress computation has been performed, an output file used to plot the effective stress field $\sigma_{\mathrm{eff}}(\boldsymbol{x})$ directly in the FE-software Ansys is generated. From the effective stress plot, it is possible to identify hot-spots and other highly stressed regions that contribute to the component's fatigue risk. By plotting the effective stress field over the component geometry, information about how to re-design a component in order to decrease the fatigue risk is obtained.

In order to account for variation in the material's fatigue properties and compute the failure probability p_f for the component, the effective fatigue stress field, $\sigma_{\text{eff}}(\boldsymbol{x})$, is used either in WL, see Eq. 2, or in the newly developed VPF[9]. In VPF, the failure probability p_f is obtained as function of the highly stressed volume V^*,

$$p_f = 1 - \exp[-q \cdot \langle V^* - V_{\text{th}} \rangle], \qquad (13)$$

where q is a material parameter and V_{th} is a threshold volume. The highly stressed volume V^* is defined as the volume in which $\sigma_{\text{eff}} > \sigma_{\text{th}}$, where σ_{th} is a threshold stress. If the highly stressed volume V^* is below the threshold volume V_{th}, the failure probability $p_f = 0$. The threshold volume V_{th} can be interpreted as an *ad-hoc* stress gradient adjustment.

In AROMA-PF, the volume integration in Eq. 2 and Eq. 13 is performed numerically by use of the effective stress that acts at the elements´ Gauss points and standard Gauss integration. The volume integration has been implemented in AROMA-PF for all quadratic solid elements typically used in industry for stress analysis: 20-noded brick elements, 15-noded prism elements, 13-noded pyramid elements and 10-noded tetrahedral elements. For WL, the failure probability p_f for a model with N_{E} finite elements is computed according to

$$p_f = 1 - \exp\left[-\frac{1}{V_0}\sum_{i=1}^{N_{\text{E}}}\sum_{j=1}^{N_{\text{G}}}\left\{\left(\frac{\langle \sigma_{\text{eff}}(\boldsymbol{x}) - \sigma_{\text{th}} \rangle}{\sigma_0}\right)^b J \cdot w\right\}_{ij}\right], \qquad (14)$$

where J is the determinant of the Jacobi matrix, w is the Gauss weight and N_{G} is the number of Gauss points in element i. The failure probability p_f for the V^*-model is computed according to

$$p_f = 1 - \exp\left[-q \cdot \langle \sum_{i=1}^{N_{\text{G}}^*} \{J \cdot w\}_i - V_{\text{th}} \rangle\right], \qquad (15)$$

where N_{G}^* is the number of Gauss points stressed above the threshold stress σ_{th}.

5. Transferability for WL and VPF

Uniaxial fatigue tests have been performed for hourglass shaped cylindrical Ti-6-4 specimens at the stress ratios R = -1, 0.1 and 0.55, and for single notched cylindrical specimens at the stress ratios R = -1 and 0.1. The elastic stress concentration factor for the notched and the smooth specimens is $K_t = 1.89$ and $K_t = 1.02$, respectively. The specimen geometries are presented in Figure 3.

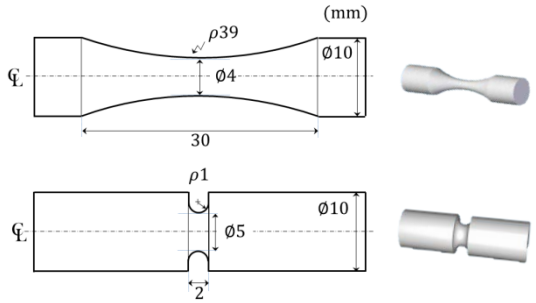

Figure 3. Specimen geometries.

For each stress ratio R, tests are performed at two stress levels. Several tests are performed at each stress level, and from the test results the experimental failure probability, p_f^{exp}, is estimated.

The test results are presented in Table 1. In Table 1, σ_{nom} is the nominal stress, n is the number of specimens tested at a certain stress level and k is the number of failed specimens. The failure probability p_f^{exp} is estimated as the median ranked failure probability.

Table 1. Experimental results.

i	K_t	R	σ_{nom} (MPa)	n	k	p_f^{exp}
1	1.89	−1	±270	8	2	0.20
2	1.89	−1	±300	8	7	0.80
3	1.89	0.1	229 ± 188	8	4	0.44
4	1.89	0.1	237 ± 193	8	8	0.92
5	1.02	−1	±500	8	2	0.20
6	1.02	−1	±534	8	6	0.68
7	1.02	0.1	358 ± 292	6	2	0.26
8	1.02	0.1	385 ± 315	6	6	0.89
9	1.02	0.55	602 ± 175	8	4	0.44
10	1.02	0.55	640 ± 186	8	8	0.92

By use of Sines´ and Crossland´s criteria for computation of the effective stress $\sigma_{\text{eff}}(\boldsymbol{x})$, the material parameters in WL and VPF are determined by minimizing the total error, e^2, between experimental results and model predictions for all 10 stress levels,

$$e^2 = \sum_{i=1}^{10}\left[p_{f,i}(\boldsymbol{\theta}) - p_{f,i}^{\text{exp}}\right]^2, \qquad (16)$$

where $\boldsymbol{\theta}$ is a parameter vector. For WL, when Sines´ criterion is used for computation of $\sigma_{\text{eff}}(\boldsymbol{x})$ and when the reference volume $V_0 = 1$ mm³, the optimal set of parameters becomes $\sigma_{\text{th}} = 0$ MPa, $\sigma_0 = 593$ MPa, $b = 28.8$ and $\alpha_{\text{S}} = 1.67$, with the corresponding total error $e^2 = 0.723$. For VPF, the optimal choice of parameters is $\sigma_{\text{th}} = 538$ MPa, $V_{\text{th}} = 0.692$ mm³, $q = 1.74$ mm^{-3} and $\alpha_{\text{S}} = 1.74$, with the corresponding total error $e^2 = 0.859$. In Figure 4, by use of the optimal sets of parameters, the failure probabilities obtained by use of WL and VPF are plotted as function of the maximum nominal stress that acts in the specimen during the load cycle, and are compared to the experiments.

The smallest total error e^2 is obtained for WL. In Figure 4, it is seen that the transferability for WL and VPF is poor at stress ratio $R = -1$ (where $\sigma_{\text{h,mean}} = 0$ MPa), and that the volume effect at $R = -1$ is overestimated in the model predictions.

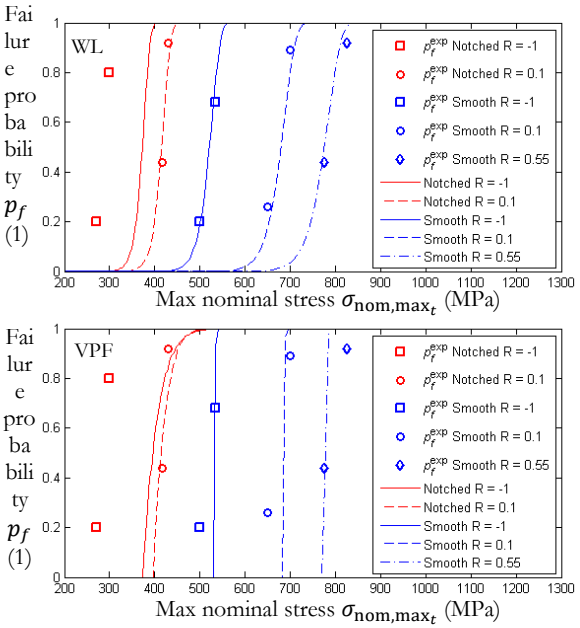

Figure 4. The best fit of WL and VPF when Sines is used for computation of $\sigma_{\text{eff}}(\boldsymbol{x})$.

In Figure 5, WL and VPF are fitted to the test data in Table 1 when Crossland´s criterion is used for computation of $\sigma_{\text{eff}}(\boldsymbol{x})$. The optimal sets of parameters that minimize the error e^2, see Eq. 16, are given in Figure 5.

Also when Crossland´s criterion is used, the smallest error, e^2, is obtained for WL. The transferability at $R = -1$ is improved compared to the results in Figure 4. However, for WL a limited transferability is now instead obtained at stress ratio $R = 0.1$. For VPF, the standard deviation of the p_f-curves in Figure 5 becomes too large for the notched specimens. In both Figures 4 and 5, when VPF is applied to the smooth specimens, the predicted failure probability increases too rapidly compared to the experiments.

In Figure 6, the error e^2 obtained for the optimal fits shown in Figure 4 and Figure 5 is given.

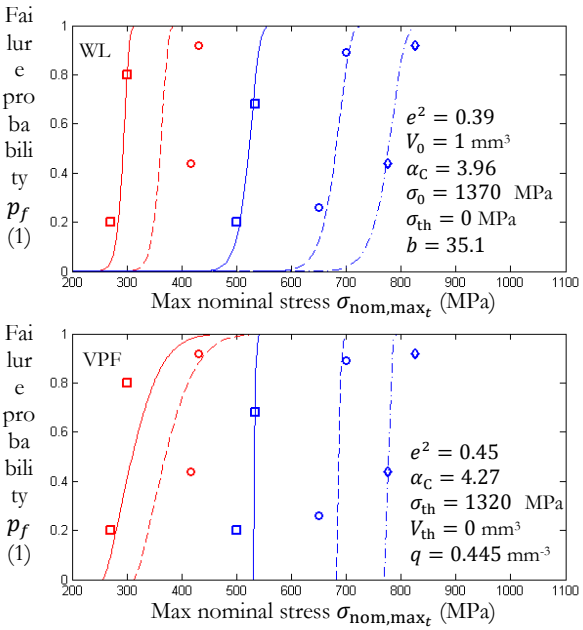

Figure 5. The best fit of WL and VPF when Crossland is used for computation of $\sigma_{\text{eff}}(\boldsymbol{x})$. The legend is the same as for Figure 4.

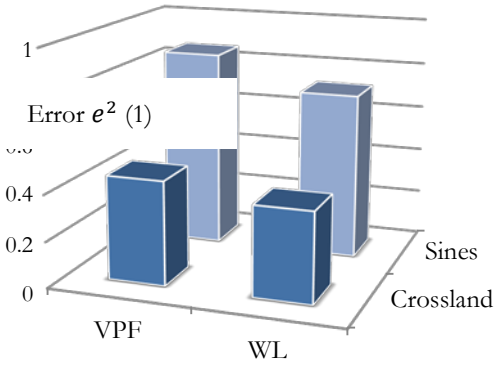

Figure 6. The error e^2 for the optimal sets of parameters.

6. AROMA-PF applied to a compressor blade

In this Section, by use of the material parameters obtained in Section 5, AROMA-PF is used to compute the failure probability p_f for a compressor blade geometry. The failure probability computations are performed by use of WL and VPF for in total three load cases, denoted LC_1, LC_2 and LC_3, respectively. Each one of the three load cases corresponds to a critical crossing in the Campbell diagram. The meshed compressor blade geometry is presented in Figure 7. The blade is meshed by use of solid elements with quadratic shape functions.

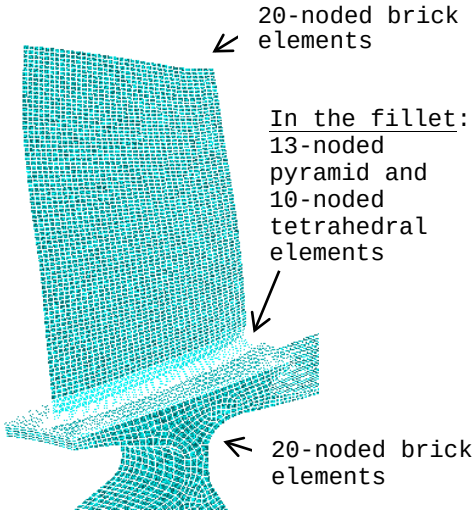

Figure 7. The meshed compressor blade geometry.

For each load case LC_1, LC_2 and LC_3, the total stress $\boldsymbol{\sigma}(\boldsymbol{x},t)$ that acts in the blade consists of a mean stress, $\boldsymbol{\sigma}_{\text{mean}}(\boldsymbol{x})$, and a varying stress, $\boldsymbol{\sigma}_{\text{amp}}^{\text{Re}}(\boldsymbol{x})\cdot\cos(\omega t)+\boldsymbol{\sigma}_{\text{amp}}^{\text{Im}}(\boldsymbol{x})\cdot\sin(\omega t)$, see Eq. 8. The mean stress $\boldsymbol{\sigma}_{\text{mean}}(\boldsymbol{x})$ is caused by rotation (with angular frequency ω) and a steady pressure applied to the blade's pressure side, and is obtained from a static FE-analysis. The steady stress field is presented in Figure 8 for each LC. As can be seen in Figure 8, the HCF analyses are performed only for the blade, including the fillet. The part of the geometry located below the fillet is excluded from the p_f-computation.

For each LC, the varying part of the total stress $\boldsymbol{\sigma}(\boldsymbol{x},t)$ is obtained from a modal analysis. The distribution of the varying part of the total stress $\boldsymbol{\sigma}(\boldsymbol{x},t)$ is given in Figure 9. The stress shown in Figure 9 is the shear stress $\sqrt{J_{2,\text{amp}}}$ computed by use of MCH.

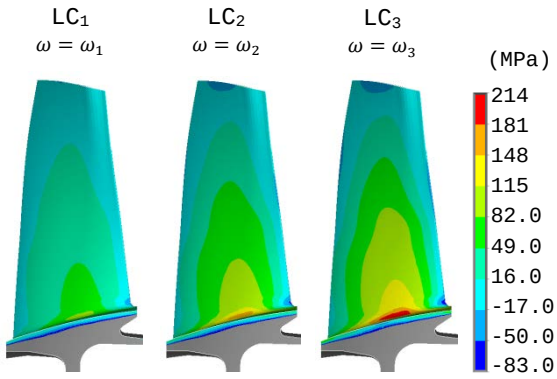

Figure 8. The mean stress plotted as hydrostatic stress, $\sigma_{\mathrm{h,mean}}(\boldsymbol{x})$. For the angular frequencies ω, the relation $\omega_1 < \omega_2 < \omega_3$ holds.

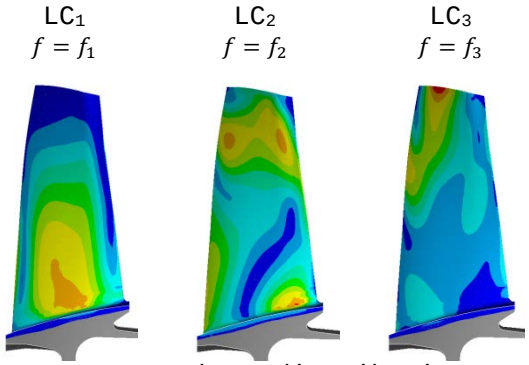

Figure 9. The distribution of $\sqrt{J_{2,\mathrm{amp}}}$, computed by use of MCH. For the vibrational frequencies, the relation $f_1 < f_2 < f_3$ holds.

By use of the output from AROMA-PF it is possible to create stress-volume curves that illustrate the distribution of the effective stress in the component. In Figure 10, the vibrational amplitude has been scaled such that the same maximum Crossland effective stress $\sigma_{\mathrm{eff,C,max}_{\boldsymbol{x}}} = 1200$ MPa ($\alpha_{\mathrm{C}} = 3.96$) acts in the blade for each LC. It is seen that even if the maximum effective stress is the same, the effective stress distribution over the volume in the blade differs between the three load cases.

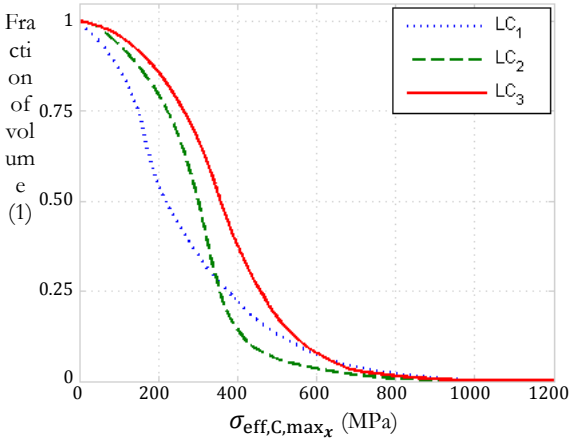

Figure 10. The stress-volume curves for the effective stress field when $\sigma_{\mathrm{eff,C,max}_{\boldsymbol{x}}} = 1200$ MPa in each LC.

For each LC, by scaling for example the blade's vibrational amplitude, AROMA-PF can be used to plot the failure probability as function of the maximum effective stress, $\sigma_{\mathrm{eff,max}_{\boldsymbol{x}}}$, that acts in the blade. In WL and VPF, the failure probability p_f is computed from a volume integration of the effective stress field. Therefore, due to the difference in effective stress distribution in the blade between each LC, for a certain maximum effective stress $\sigma_{\mathrm{eff,max}_{\boldsymbol{x}}}$, there is a difference in the predicted failure probability between each LC. For example, when Crossland´s criterion is used for computation of σ_{eff}, for the maximum effective stress $\sigma_{\mathrm{eff,C,max}_{\boldsymbol{x}}} = 1200$ MPa, the failure probability for LC_1, LC_2 and LC_3 according to WL is predicted to $p_f = 1.8 \cdot 10^{-2}$, $p_f = 5.6 \cdot 10^{-3}$ and $p_f = 3.7 \cdot 10^{-2}$, respectively, see Figure 11. For VPF, since the threshold stress $\sigma_{\mathrm{th}} = 1320$ MPa when Crossland´s criterion is used, the failure probability $p_f = 0$ for each LC at stress level $\sigma_{\mathrm{eff,C,max}_{\boldsymbol{x}}} = 1200$ MPa.

The results in Figure 11 show that for all three load cases, when Crossland´s criterion is used for computation of the effective stress, WL is more conservative

than VPF. It is also seen that for low failure probabilities, the slope of the p_f-curves generated by use of VPF is higher compared to the slope of the p_f-curves generated by use of WL.

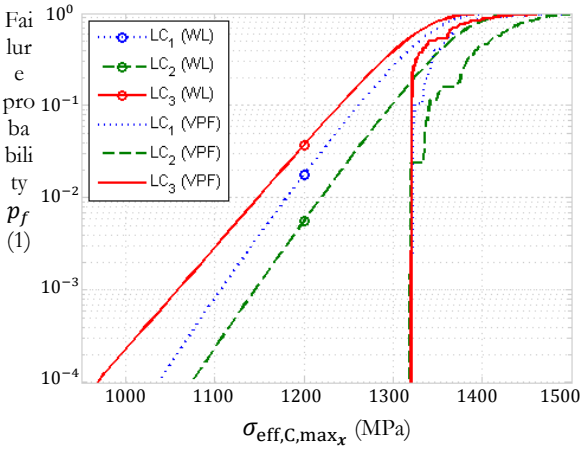

Figure 11. The failure probability due to uncertainty only in the material's fatigue properties as function of the maximum effective stress $\sigma_{\mathrm{eff,C,max}_x}$.

If instead Sines´ criterion is used for computation of the effective stress field, the fatigue probability predictions obtained for the compressor blade by use of VPF becomes more conservative than the WL predictions at high p_f-values, see Figure 12. At low p_f-values, WL is more conservative than VPF.

In Figure 12, for LC_2, similar to when Crossland´s criterion is used, the slope of the p_f-curve generated by use of VPF is higher at low p_f-values compared to the slope of the p_f-curve generated by use of WL. For LC_1 and LC_3, the slope of the p_f-curves generated from VPF is higher than the slope of the corresponding p_f-curves obtained by use of WL over basically the whole p_f-interval. In Figure 12, the effect of a threshold volume $V_{\mathrm{th}} > 0$ is also seen; the p_f-curves generated from VPF do not approach $p_f = 0$ for the same stress value.

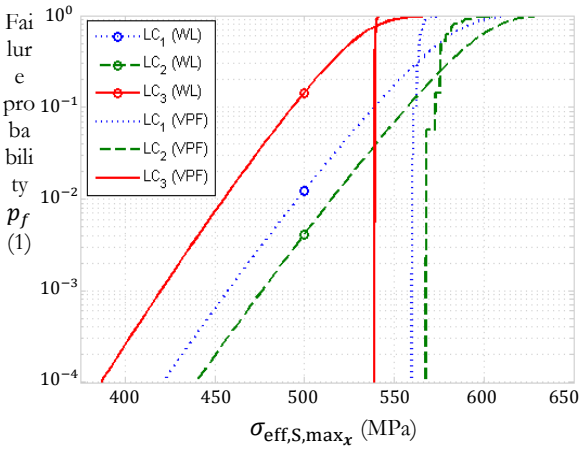

Figure 12. The failure probability due to uncertainty only in the material's fatigue properties as function of the maximum effective stress $\sigma_{\mathrm{eff,S,max}_x}$.

7. Discussion and conclusions

As seen in Figures 8 and 9, depending on the vibrational mode shape, points subjected to high values of amplitude stress may be located in regions with either low or high steady hydrostatic stress. Therefore, the prediction accuracy for WL and VPF is important at each R-value shown in Figures 4 and 5.

The material´s true fatigue behavior at low p_f-values is difficult and time consuming to estimate. From Figures 11 and 12, it is seen that use of VPF gives a fatigue behavior that probably is too deterministic. On the other hand, the curves generated by use of WL gives a long lower tail. It seems reasonable to believe that the material´s true fatigue behavior at low p_f-values is between the predictions obtained by use of WL and VPF.

In a probabilistic based design setup, the aim is to identify and model each contribution to the overall uncertainty that affects

the component's fatigue risk p_f^{tot}. The inherent variation in the material's fatigue properties is only one of the contributions to the overall uncertainty, see Figure 1. Work is ongoing, to implement AROMA-PF in a design tool that includes various technical disciplines involved in compressor blade design. The goal is to include all uncertainties and compute the total failure probability p_f^{tot}. This enables reliability based design.

The work is summarized and concluded as follows:

- For stress invariant based local HCF criteria, a closed form expression for the effective stress when there is a difference in phase between the stress components has been derived. This enables fast HCF evaluations.
- The HCF post-processor AROMA-PF, with several local multiaxial HCF criteria and two probabilistic HCF models implemented, has been presented.
- Based on experimental data obtained for the typical gas turbine material Ti-6-4, it is shown that use of Crossland´s HCF criterion in combination with WL gives the smallest total error between experiments and model predictions.
- The material´s true fatigue behavior at low p_f-values is probably between the predictions obtained by use of WL and VPF.

8. Acknowledgement

This work has been promoted by the Swedish Energy Agency Authority through TURBOPOWER. This financial support is gratefully acknowledged. The cooperation with GKN Aerospace and Siemens Industrial Turbomachinery AB is also acknowledged.

9. References

[1] Findley W.N. A theory for the effect of mean stress on fatigue of metals under combined torsion and axial load or bending. J Eng Ind 1959:301-6.

[2] Matake T. An explanation on fatigue limit under combined stress. Bull JSME 1977; 20(141):257-63.

[3] Dang Van K. Macro-micro approach in high-cycle multiaxial fatigue. In: McDowell DL, Ellis R, editors. Advances in multiaxial fatigue. ASTM STP 1191. Philadelphia: American Society for Testing and Materials; 1993. p. 120–30. ISSN 0066-0558.

[4] Sines G. Behavior of metals under complex static and alternating stresses. In: Sines G. & Waisman J.L, editors. Metal Fatigue. New York: McGraw-Hill; 1959. p. 145-69.

[5] Crossland B. Effect of large hydrostatic pressure on the torsional fatigue strength of an alloy steel, in: Proceeding of International Conference on Fatigue of Metals, London & New York; 1956. p. 138–49. ISBN 99-0981150-2.

[6] Weibull W. A statistical theory of the strength of materials, Handlingar Ing.vetenskapsakademien; 1939. No. 151. ISBN 991- 428078-1.

[7] Sadek S, Sandberg D, Olsson M. FE-mesh effect of the volume based weakest-link fatigue probability applied to a compressor blade. In: Proceedings of the ASME Turbo Expo. vol. 7, Issue PARTS A AND B; 2012. p. 427–38.

[8] Papadopoulos I.V, et. al. A comparative study of multiaxial high-cycle fatigue criteria for metals. Int J Fatigue 1997; 19(3):219-35.

[9] Sadek S, Olsson M. New models for prediction of high cycle fatigue failure based on highly loaded regions. Int J Fatigue 2014; 66:101–10.